ARTICLE

Single Droplet Break-up in Controlled Mixed Flows

Elia Boonen, Peter Van Puyvelde,* and Paula Moldenaers

Department of Chemical Engineering and Leuven Materials Research Centre, Katholieke Universiteit Leuven, Willem de Croylaan 46, B-3001 Leuven (Heverlee), Belgium

ABSTRACT In this work, the break-up dynamics of a single, Newtonian droplet dispersed in an immiscible Newtonian matrix undergoing a controlled mixture of shear and extensional flow is investigated using a homemade eccentric cylinder device. Hereto, different representative supercritical flows with varying shear/elongation balance have been applied. The effect of viscosity ratio is explored using droplets with a viscosity ratio of 0.1 and 1.3, respectively. In all cases, break-up is observed to proceed through an "end-pinching" mechanism. The experimentally obtained break-up times have been compared with scaling relations known from literature for simple shear and purely extensional flow. It is found that the global break-up dynamics is still shear dominated, even for conditions where the elongational contribution comprises a substantial amount (up to 30% on average) of the mixed flow.

KEYWORDS: break-up • polymer blends • single droplets • mixed flows • eccentric cylinders

INTRODUCTION

Dispersing one fluid in a second immiscible liquid is an important unit operation associated with many industrial processes as encountered in food processing, pharmaceuticals manufacturing, and polymer blending. A profound understanding of the morphology development during such mixing flows requires elucidation of the underlying processes including break-up and coalescence of drops. Because single droplet dynamics are discussed in this paper, we will limit the discussion here to the break-up process.

Break-up of single, Newtonian droplets has been the subject of many investigations since the pioneering work of Taylor (1, 2). An extensive review is given by Tucker and Moldenaers (3), and Guido and Greco (4). Usually, four different break-up mechanisms can be distinguished (5); when the flow strength is gradually increased, a single droplet is split up into two equal-sized daughter drops by necking in the middle part, the so-called binary break-up (6). Capillary wave break-up, on the other hand, occurs when a very strong flow is applied in which the drop has no time to adapt its shape. As a result, a highly elongated thread is formed on which sinusoidal perturbations (Rayleigh instabilities) develop that lead to break-up into a string of smaller droplets. This mode of break-up was also theoretically investigated by several researchers (7−9). The third type of break-up is the end-pinching mechanism as described by Stone et al. (10−12), which can occur after cessation of a strong flow (10) or after step changes in flow rate and/or flow type (12). Here, under the action of the interfacial tension, a sufficiently stretched filament will form bulbous ends which grow larger and pinch off from the center waist of the drop. Finally, tip streaming is a break-up mechanism whereby small drops are released from the pointed ends of a parent drop (13). This is however, not a general break-up mechanism and can mostly be attributed to the presence of impurities or a nonuniform surfactant distribution along the drop surface (14, 15). Other break-up mechanisms have been described in literature, for instance when dealing with viscoelastic components (16, 17) or when using microfluidic devices in which confinement effects become important (18, 19). Here, however, we focus on bulk behavior of systems with Newtonian components.

Most of the former break-up studies considered either simple shear or pure extensional flow. In real processing flows, a complex and transient flow field is encountered combining shear and extension. Only a few studies deal with "mixed-flow" conditions in which a controlled combination of shear and extensional flow is applied. Han and Funatsu (20) studied the deformation of single droplets in a complex flow field using a sudden contraction. They observed that fibril break-up occurs by capillary instabilities but only after entering the contraction. Comparable results were obtained by Chin and Han (21) and Van der Reijden-Stolk and Sarah (22), who used a gradually converging channel. One limitation of these studies is that the droplet size was comparable to the transverse dimension of the flow field. Under such conditions, confinement effects might interfere with the conclusions (23, 24). Godbille and Picot (25) and Khayat and co-workers (26) also documented this when studying the influence of shear and elongation on drop deformation and break-up in convergent-divergent flows. Furthermore, they identified different break-up mechanisms driven by extension and shear flow respectively, for this specific geometry. For instance, shear driven double tip streaming was observed in some cases causing break-up into very fine droplets formed behind the main drop. Similar results were

* Corresponding author. E-mail: Peter.Vanpuyvelde@cit.kuleuven.be. Tel: +32-16-32.23.57. Fax: +32-16-32 0.29.91.
Received for review May 3, 2010 and accepted June 23, 2010

DOI: 10.1021/am100389x

Published on Web 07/12/2010

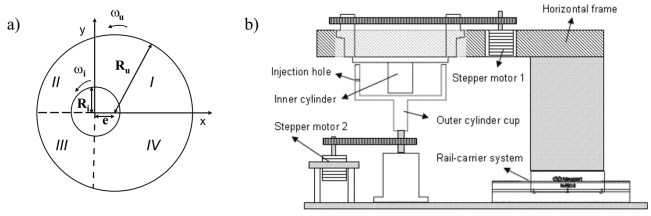

FIGURE 1. (a) Sketch of top view of eccentric cylinder system. (b) Schematic of eccentric cylinder device.

obtained by Mietus et al. (27) for the confined shear and extensional flows produced in a horizontal Couette cell with local inserts. They discerned a number of interesting and more complex droplet configurations, including "clawlike", "swallow-tail", and "horseshoe-crab" structures.

More concentrated blends were used by Testa et al. (28) to study the morphology development after a sudden contraction and in a gradually converging channel followed by a sudden expansion. The flow-induced morphological evolution could be predicted, at least semiquantitatively, by assuming that the effects of extension and shear are additive. These authors state, based on their experiments, that droplet break-up takes place when either the local shear or stretching rate, averaged over the thickness of the flow channel, exceeds the critical value for break-up as obtained from steady homogeneous flow data. Similar conclusions were drawn by Priore and Walker (29) based on small-angle light-scattering experiments. The conclusions drawn by Testa et al. and Priore and Walker were, however, focused on observations along the centerline of the geometry. Hence, their flows are dominated by elongation, thus limiting to a certain extent the applicability of their results to real complex flows. Oosterlinck et al. (30) on the other hand, studied the morphology development of a dilute polymer blend in capillary flow, for droplets moving on as well as off the die axis. They verified that the Tomotika theory could qualitatively describe the break-up behavior, occurring through Rayleigh instabilities in both cases. For fibrils flowing off center though, the actual shear thinning viscosities have to be used.

Earlier, Bentley and Leal (31) used a computer controlled four-roll mill to study droplet deformation and break-up in steady flows ranging between simple shear and 2D-elongation. They provide a systematic data set of critical conditions for (binary) droplet break-up in these intermediate flow types. Later on, Stone and co-workers (10, 12) proceeded with the same geometry to study transient effects in droplet dynamics upon cessation of flow and after step changes in the flow type and/or flow intensity. Despite its flexibility, the four-roll mill suffers from flow instabilities, which render it difficult to center droplets in the flow field.

Alternatively, controlled mixed flow conditions can also be applied using an eccentric cylinder system (see Figure 1a). This flow geometry has been well-studied in the area of lubrication phenomena occurring in journal bearings (32−34). Ottino and co-workers (35−37) were the first to employ the flow generated between eccentric cylinders to disperse one fluid into another. They investigated the dynamics of droplet elongation, folding and break-up in chaotic flows produced between the two cylinders. In particular, Tjahjadi and Ottino (37) observed that the dominant break-up mechanism is through capillary wave instabilities in highly stretched filaments. Recently, the eccentric cylinder geometry has received renewed interest by Windhab and co-workers (38−40). Feigl et al. (38), for instance, combined a numerical and experimental approach to study drop break-up when only the inner cylinder rotates at a constant speed. In this specific case, however, the elongational strain rates are less than 1 % of the shear rates. Therefore, the break-up can be considered to be shear dominated in their investigations.

Our research focuses on the morphology development of immiscible polymer blends in controlled mixed flow conditions. For this purpose, a new eccentric cylinder device (ECD, see Figure 1b) that provides a balanced mixture of shear and elongational components, has been designed and validated previously (41). In the present work, we investigate the break-up process in some representative supercritical mixed flows applied with the ECD. This includes a study of the mode of break-up as well as break-up times.

THEORY

For a system with matching fluid densities and Newtonian components, the only two dimensionless parameters that govern the droplet dynamics in slow flows are the viscosity ratio $p = \eta_d/\eta_m$ with η_d the viscosity of the drop fluid and η_m the viscosity of the matrix, and the capillary number *Ca*, which represents the ratio of hydrodynamic stresses that tend to distort the spherical shape of a droplet over the interfacial stresses that try to restore its original shape. Hence, *Ca* is defined as $(\eta_m R_0 E)/\Gamma$, where R_0 is the radius of the undistorted spherical droplet and Γ is the interfacial tension. *E* is a parameter that represents the velocity gradient. Actually, it is defined as the second scalar invariant of the rate of deformation tensor $\bar{\bar{D}}$ (42). In simple shear flow, *E* equals the shear rate $\dot{\gamma}$, whereas in extensional flow, the strain rate $\dot{\varepsilon}$ is used. In complex flows, however, both shear as well as extensional components are present. In the present case, the rate of deformation tensor can be written as (43)

$$\begin{pmatrix} \dot{\varepsilon} & \frac{\dot{\gamma}}{2} & 0 \\ \frac{\dot{\gamma}}{2} & -\dot{\varepsilon} & 0 \\ 0 & 0 & 0 \end{pmatrix}$$

Hence, for this two-dimensional complex flow, the second scalar invariant *E* can be calculated to be

$$\sqrt{4\dot{\varepsilon}^2 + \dot{\gamma}^2}$$

For steady flows, a critical capillary number Ca_{crit} exists above which a droplet breaks up. This critical capillary number depends on the viscosity ratio *p* and the flow type (44). The latter can be represented by the flow type param-

eter $\bar{\alpha}$, as defined by Feigl et al. (38) and which represents the relative amount of elongation present in the flow field

$$\bar{\alpha} = \frac{\dot{\varepsilon}}{|\dot{\gamma}| + |\dot{\varepsilon}|} \quad (1)$$

with $-1 \leq \bar{\alpha} \leq 1$. Mixed-flow conditions between eccentric cylinders can thus be represented by E and $\bar{\alpha}$. Pure shear flow corresponds to $\bar{\alpha} = 0$, pure 2D elongation to $\bar{\alpha} = 1$. In general, the strain rates will vary in time along a certain streamline, giving rise to a time dependent capillary number $Ca(t)$ and flow type parameter $\bar{\alpha}(t)$.

For steady simple flows, it is known that the total break-up time t_b (after start-up of the flow) obeys the following scaling behavior (45, 46)

$$t_b\dot{\gamma} \approx \left(\frac{\eta_m R_0 \dot{\gamma}}{\Gamma}\right)^{2/3} p^{0.5} \text{ and } t_b\dot{\varepsilon} \approx \log\left(\frac{\eta_m R_0 \dot{\varepsilon}}{\Gamma}\right) p^{0.5} \quad (2)$$

for simple shear and extensional flow, respectively. Thus, the dimensionless break-up time for either simple shear or extension scales with a certain function of the capillary number Ca and the viscosity ratio p. The scaling function for Ca was derived from the original Khakhar and Ottino theory (9) for break-up in steady linear flows and verified experimentally. The scaling with $p^{0.5}$, on the other hand, was empirically found by Van Puyvelde et al. (45).

For the mixed flows obtained in the ECD, it is not straightforward anymore to make the experimental break-up time dimensionless. One can make time dimensionless by using the second scalar invariant of the rate of deformation tensor. However, here we will also make time dimensionless with the flow strength $G_{B\&L}$ as defined by Bentley and Leal (31)

$$G_{B\&L} = \frac{\sqrt{4\dot{\varepsilon}^2 + \dot{\gamma}^2}}{1 + \alpha_{B\&L}} \text{ with } \bar{\alpha} = \frac{\sqrt{\alpha_{B\&L}}}{1 - \alpha_{B\&L} + \sqrt{\alpha_{B\&L}}} \quad (3)$$

Here, $\alpha_{B\&L}$ is the flow type parameter used by Bentley and Leal, which is always larger than zero and can be expressed as a function of our flow parameter $\bar{\alpha}$. $G_{B\&L}$ is used instead of E because it recovers the extensional case (for $\alpha_{B\&L} = \bar{\alpha} = 1$; $G_{B\&L} = \dot{\varepsilon}$). Finally, to compare the break-up behavior for the transient mixed flows with the scaling laws of eq 2, the problem arises that $G_{B\&L}$ and Ca will vary in time. Therefore, we propose to use average values $G_{B\&L}^{avg}$ and Ca^{avg} over one rotation of the ECD.

MATERIALS AND METHODS

Poly(isobutylene) (PIB, Glissopal 1300), with a viscosity of 51.6 Pa.s at room temperature (~23 °C), is chosen as the matrix phase, whereas two grades of poly(dimethylsiloxane) (PDMS, Rhodorsil) with viscosities of 60.4 and 5.10 Pa.s have been selected as the droplet phase resulting in viscosity ratios p of 0.1 and 1.3. All fluids are transparent at room temperature and exhibit Newtonian behavior over the range of strain rates investigated here. The interfacial tension Γ of the PDMS/PIB system is 2.8 ± 0.1 mN/m and was reported to be independent of the molecular weight (M_w) for the grades used here (41). All experiments were performed at ambient temperature. As the viscosity of PIB is very sensitive to temperature, the temperature of the sample was directly monitored by inserting a fine thermocouple needle in the continuous phase. Hence, the viscosities η_m and η_d, and the resulting viscosity ratio p, could be back-calculated using an Arrhenius equation.

Table 1. Configurations of ECD Used in This Work

configuration	shear dominated flow	enhanced extensional component flow
eccentricity ratio X	0.2	0.2
velocity ratio ω_i/ω_u	0	2/3
$\bar{\alpha}^{avg,I-II}$	0.10	0.30

The controlled mixed-flow conditions are applied using a custom-built ECD as depicted in Figure 1, which is described in more detail elsewhere (37). In brief, the device is capable of applying a combination of shear and extensional flow in the annular gap between two cylinders. The inner and outer cylinders, with radii R_i and R_u and angular velocities ω_i and ω_u, can be displaced by a distance e, the eccentricity. The eccentricity ratio X is then defined as $e/(R_u - R_i)$. For the experiments presented here, the ECD has been used in two rotation modes to vary the balance of shear and elongational flow components: a shear dominated flow in which only the outer cylinder rotates with a constant speed, and a flow with an *enhanced extensional contribution* where both cylinders are corotating with the ratio of inner to outer cylinder velocity $\omega_i/\omega_u = 2/3$. In both cases the eccentricity ratio X is set to a value of 0.2. The two configurations of the ECD are summarized in Table 1. In the enhanced extensional mode, an extensional contribution of 30% is reached. Increasing this value even further is possible, but under such conditions a recirculation vortex can become present that would interfere with a droplet traveling on a streamline. In the experimental procedure, single PDMS droplets with initial radii in the range of 400−800 μm were introduced in the matrix material by means of a homemade injection system. The droplets are small enough to be able to neglect confinement effects (23). The spherical drop is injected in the widest part of the gap at a radial distance of about 30 mm (half the clearance) from the axis of the inner cylinder. Subsequently, the flow is started with chosen values for ω_u and ω_i and the droplet is visualized using optical microscopy during many revolutions until the first instance of break-up (= detachment of part of the drop), which marks the break-up time. Hereto, a microscope, equipped with a CCD camera, is mounted on top of the flow cell to capture images of the deforming drop. Because of the limited field of view of the microscope and difficulties in illumination, images of the deforming drop could, for each single experiment, only be captured in the first two (I and II) or the last two (III and IV) quadrants of the Cartesian coordinate system, defined in Figure 1a. Furthermore, to explore different ranges of Ca, we have varied the rotational speeds as well as the initial droplet size R_0.

RESULTS AND DISCUSSION

Break-up Mode. In the controlled complex flows applied here, the shear and elongational strain rates vary in time along a streamline. A typical profile for two droplet revolutions is given in Figure 2 for the shear dominated flow. It shows that both the shear and the elongation rate are periodic in time, with clear minima and maxima appearing during one revolution. These strain rate profiles will result

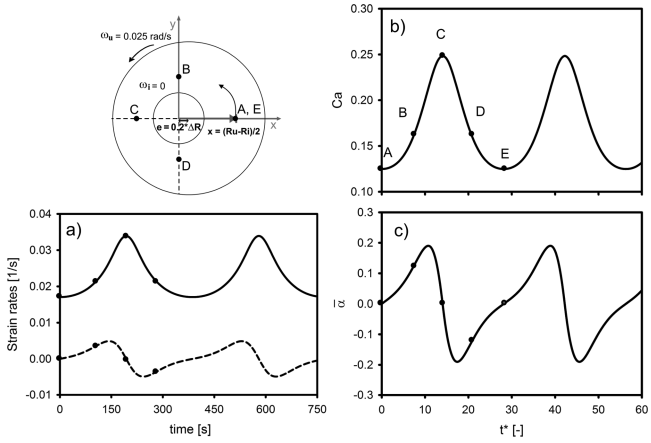

FIGURE 2. Example of flow parameters for shear dominated flow with $\omega_i = 0$, $\omega_u = 0.025$ rad/s, and eccentricity ratio $X = 0.2$, along streamline starting at $x = 30$ mm from the axis of the inner cylinder: (a) strain rate profiles, shear (-) and elongation (--) (b) evolution of *Ca*, (c) profile for $\bar{\alpha}$ (PDMS drop with initial radius of 400 μm at 23 °C).

in a time dependent capillary number *Ca* and flow type parameter $\bar{\alpha}$, as depicted in panels b and c in Figure 2. Here, t^* is time made dimensionless with the characteristic emulsion time which is defined as $\tau = \eta_m R_0/\Gamma$. This time scale represents the inherent response time of the droplets, which is inversely proportional to the interfacial tension and proportional to the matrix viscosity. Clearly, a shear dominated type of mixed flow is obtained with the average value of $\bar{\alpha}$ over quadrants I−II ($\bar{\alpha}^{avg,A-C}$) equal to 0.10, meaning that the flow comprises only 10% of extensional components. This is also evident from the *Ca* profile, which reflects the evolution of the shear rate, reaching a sharp maximum at the narrowest area of the gap (point C), and a broad minimum in the widest part of the gap (points A, E).

The droplet dynamics during shear dominated flows for a viscosity ratio of $p \approx 1.3$ are exemplified in Figure 3. In Figure 3a, typical profiles for the length L of the droplet (made dimensionless with the droplet diameter $2R_0$) are shown for sub- and supercritical flows. The experiments are characterized by the time averaged (over one period of rotation) capillary number Ca_{avg}, and observations have only been made in the first two quadrants of the flow field, as defined in Figure 1a. For the lowest *Ca* ($Ca_{avg} = 0.517$), conditions are just below critical and the droplet length exhibits a steady, oscillatory behavior as also described in our previous work (41, 47). For supercritical conditions (e.g., for $Ca_{avg} = 0.625$ in Figure 3a), the droplet length keeps increasing, though in an nonmonotonic manner, until eventually drop break-up occurs. The process resembles an undamped oscillatory behavior, and can be attributed to the time periodic applied capillary numbers *Ca* and the changing of sign of the elongation rate $\dot{\varepsilon}$ between quadrants II and III; as the *Ca* number drops at the end of quadrant II (after point C, see Figure 2b) the driving force for deformation is diminished. Furthermore, the flow type parameter $\bar{\alpha}$ becomes negative here, which means there is also a compression part in the direction of flow.

The break-up process itself is shown in more detail in Figure 3b, where the evolution of the droplet near the end

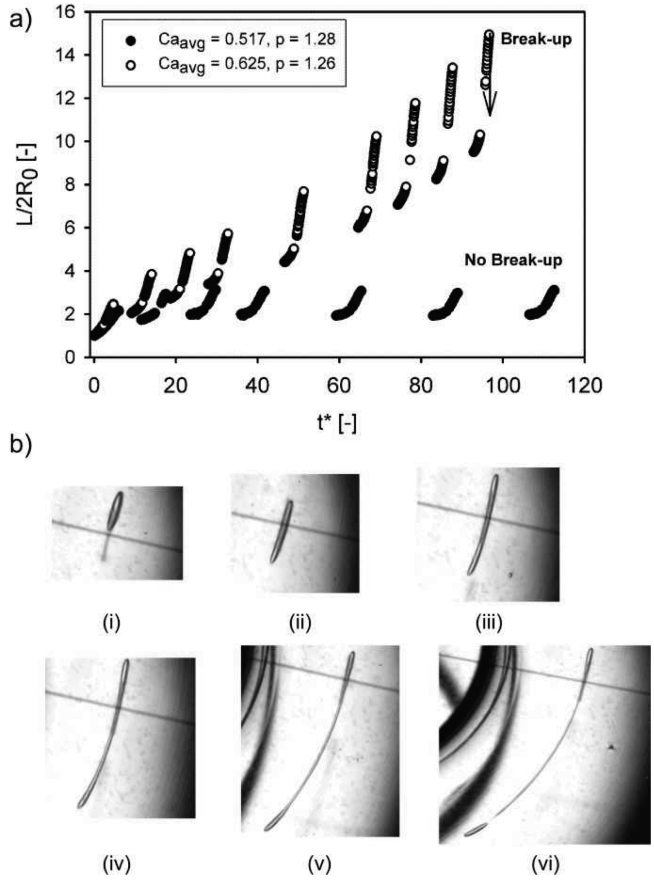

FIGURE 3. (a) Dimensionless droplet length $L/2R_0$ as a function of dimensionless time t^* for sub- and supercritical shear dominated flows of Figure 2. (b) Evolution of droplet near end of quadrant II (point C in Figure 2) for experiment with $Ca_{avg} = 0.625$: (i) $t^* = 5.00$, (ii) $t^* = 14.78$, (iii) $t^* = 34.67$, (iv) $t^* = 54.36$, (v) $t^* = 73.79$, and (vi) $t_b^* = 93.31$. Droplets with a viscosity ratio of $p \approx 1.3$.

of quadrant II is shown for the experiment with $Ca_{avg} = 0.625$ of Figure 3a. The mode of break-up observed resembles the "end-pinching" mechanism, also seen in simple shear flow (48): the droplet is progressively stretched (albeit in an oscillating manner) into a slender thread with two bulbous ends pinching off from the middle part until eventually one (or both) ends detach and droplet break-up is a fact. In this specific case for $p \approx 1.3$, the back of the drop always appears to break off first. This is probably due to the fact that the front and back of the drop "feel" different strain rates. Therefore, there can be some time delay between the response of the head and tail of the droplet, depending on the material deformation time scale (e.g., reflected in the value of p).

To investigate the effect of viscosity ratio and extend the range of break-up times (see Break-up Times section), we also studied the break-up of droplets with a viscosity ratio around 0.1 in shear dominated mixed flow. The break-up behavior was found to be very similar to the case for $p \approx 1.3$; break-up also occurs through end-pinching, though in the case for $p = 0.1$, the front and back of the droplet seem to "pinch off" more or less simultaneously. This is illustrated in Figure 4, where examples of droplet break-up are shown for different Ca_{avg}. For high *Ca* numbers (Figure 4b,c), the end-pinching is clearly visible where both the front and back

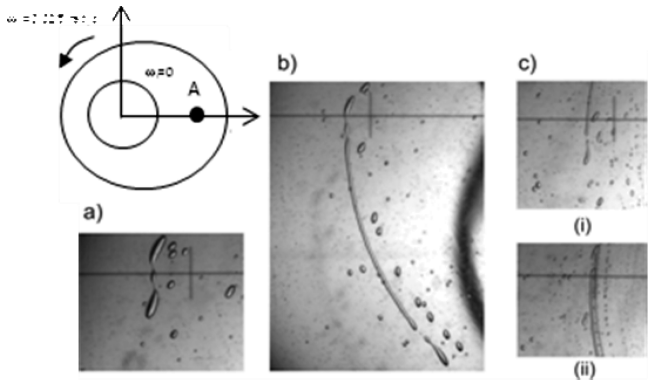

FIGURE 4. Example of droplet break-up for a viscosity ratio of $p \approx 0.1$ under flow conditions of Figure 2 at the beginning of quadrant I (point A) for: (a) $Ca_{avg} = 0.601$, (b) $Ca_{avg} = 0.878$, (c) $Ca_{avg} = 1.476$ with (i) front of drop, and (ii) back of drop.

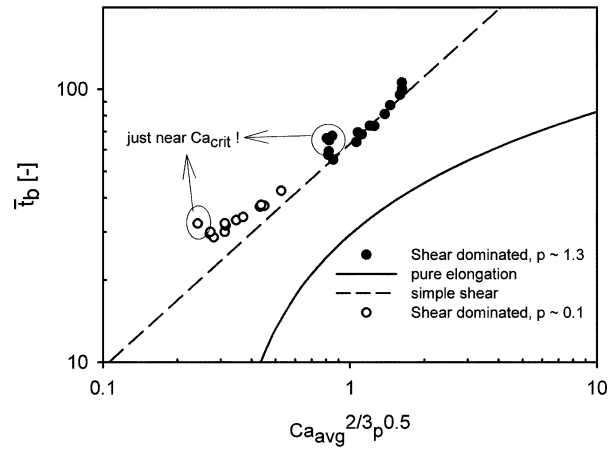

FIGURE 5. Dimensionless break-up times in mixed flow conditions of Figure 2 for a viscosity ratio p around 1.3 and 0.1. Symbols represent experimental results; lines are fits through the data of Van Puyvelde et al. (45, 49).

are detached from the rest of the droplet body. Moreover, a somewhat larger elongation is attained prior to break-up as compared to the case for $p = 1.3$. For the lowest Ca explored in Figure 4a ($Ca_{avg} = 0.601$), on the other hand, the droplet breaks up in a fashion similar to the necking phenomenon observed in steady flows (see Introduction), producing two equally sized drops with a small satellite drop in between. This mode of break-up is seen only close to the critical conditions ($Ca \approx Ca_{crit}$), where there is break-up without large scale stretching. For all other experiments performed with $p \approx 0.1$ in the shear dominated flow, break-up by end-pinching is predominant.

In a next step, the effect of varying the shear/elongation balance was investigated by studying the break-up dynamics in flows with an enhanced extensional flow component, see Table 1. In this configuration, the flow field is drastically changed as compared to the previous case, which is described in more detail elsewhere (42). In this case, the average amount of elongation $\bar{\alpha}^{avg,A-C}$ in the first two quadrants is increased to about 30% of the sum of strain rates, as compared to only 10% for the previous flow conditions.

The break-up process in this mixed flow with an enhanced extensional contribution was also studied for drops with a viscosity ratio around 1.3 and 0.1. Although the flow field is drastically changed, the break-up process was found to be very similar to the one observed in Figure 3. Under supercritical conditions, the droplet length shows an undamped oscillation until eventually break-up occurs through end-pinching, with the bulbous ends splitting off from the rest of the drop. Once again, depending on viscosity ratio p, the back of the drop can detach somewhat earlier than the front. In conclusion, the end-pinching mode can be regarded as a general break-up mechanism for the complex flows applied with the ECD.

Break-up Times. The experimentally obtained break-up times in transient mixed flows applied with the ECD, have been compared to the existing scaling laws for simple shear and purely extensional flow (see Theory section). Hereto, the dimensionless break-up time $\bar{t}_b$ is observed as a function of the average capillary number Ca_{avg} for the two viscosity ratios.

The dimensionless break-up times for droplets with a viscosity ratio around 1.3 and 0.1 in the shear dominated flows are depicted in Figure 5. Here, symbols correspond to experimental results in the ECD and break-up times have been made dimensionless with the flow strength as defined in eq 3; lines are fits through data of Van Puyvelde and co-workers (45, 49) for simple shear and extensional flow. Clearly, the break-up times for both viscosity ratios collapse with the simple shear line indicating that the break-up dynamics are shear dominated. For low p, though, a small upturn is visible, but this was also reported for steady simple shear flow (49). Only close to the critical conditions do some deviations from the scaling behavior appear to occur, as highlighted in Figure 5. This is due to the fact that just near Ca_{crit} the initial stages of the deformation process occur very slowly with respect to the total break-up process (see also Figure 3a), as also documented in literature for steady 2D flows (10).

Next, the dimensionless break-up times for mixed flows with enhanced extensional contribution are summarized in Figure 6. Again, symbols correspond to the experimental dimensionless break-up times t_b, whereas the lines are fits through data of Van Puyvelde et al. for simple flows (45, 49). Furthermore, the filled data points have been obtained by scaling with $G_{B\&L}{}^{avg}$, the open symbols represent results obtained using a different scaling factor for t_b (see Theory section), E^{avg}. When comparing open and filled symbols, it is clear that scaling the break-up times with $G_{B\&L}{}^{avg}$ or E^{avg} leads to different results in this specific flow with higher $\bar{\alpha}$ values (in contrast, for the shear dominated flows of Figure 5, there is no significant difference between the two scaling factors). Nondimensionalizing t_b with E^{avg} shifts the data up, well above the simple shear line. Hence, it seems that the correct scaling factor is $G_{B\&L}{}^{avg}$, the flow strength as defined by Bentley and Leal (31), whereas E^{avg} causes an overestimation of the flow strength contribution.

With $\bar{t}_b = t_b G_{B\&L}{}^{avg}$, the data of Figure 6 indicate again that the break-up times are shear dominated, even for this flow type with the higher values of $\bar{\alpha}^{avg,I-II}$(about 30%). For low p, a slight upturn is visible, as also seen for the shear

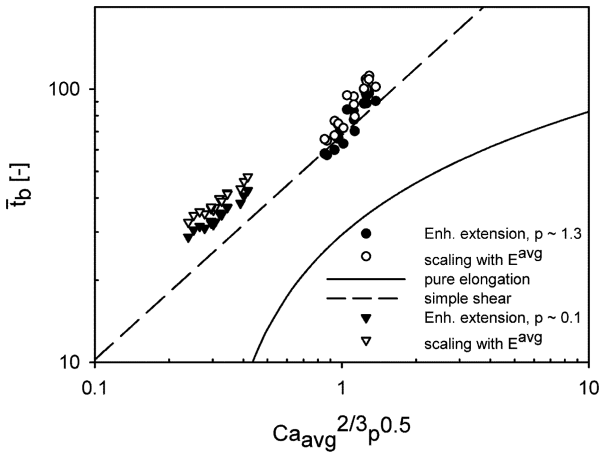

FIGURE 6. Dimensionless break-up times in mixed flow conditions with enhanced extension for a viscosity ratio p around 1.3 and 0.1. Symbols represent experimental results; lines are fits through the data of Van Puyvelde et al. (45, 49). Note that the open symbols are obtained when nondimensionalizing the break-up time t_b with the average value of the flow intensity E^{avg}, filled symbols are nondimensionalized with $G_{B\&L}{}^{avg}$.

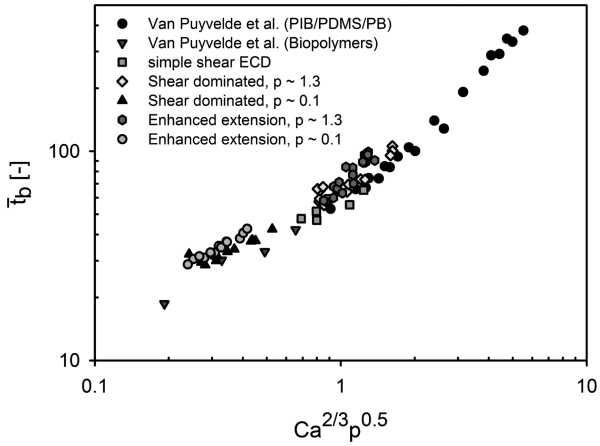

FIGURE 7. Dimensionless break-up times for all mixed flows applied with the ECD together with simple shear data from Van Puyvelde et al. (45, 49).

dominated flow conditions (Figure 5). This is more clearly seen in Figure 7, which collects all the break-up data obtained in the ECD (including simple shear data) together with the simple shear data obtained by Van Puyvelde et al. for synthetic (45) as well as biopolymers (49). Overall, the scaling is very reasonable for all data in mixed as well as simple shear flows. Hence, despite the transient nature of the mixed flows applied with the ECD, the global break-up dynamics can still be described by a simple scaling relation when using average values for the flow strength and the capillary number. Furthermore, simple shear break-up behavior is followed despite the substantial (positive and negative) elongational strain pulses present in the flow field.

CONCLUSIONS

The break-up dynamics of single Newtonian droplets immersed in a Newtonian matrix subjected to controlled mixed flows have been investigated using a homemade eccentric cylinder device. For all mixed flows applied and viscosity ratios of 0.1 and 1.3, break-up is observed to occur through an "end-pinching" mechanism where the two bulbous ends gradually detach from the slender waist of the drop. Depending on viscosity ratio p, front and back of the drop break off at different moments in time because of the transient nature of the flow. The dimensionless break-up times, based on average values for flow strength and capillary number, follow the scaling relation for steady simple shear flow reported in literature. Hence, the global break-up dynamics are still shear dominated even for mixed flows with substantial amounts of elongation (up to 30% on average) present in the flow.

Acknowledgment. Onderzoeksfonds K.U. Leuven (Grants GOA 03/06 and GOA 09/002) is gratefully acknowledged for financial support.

REFERENCES AND NOTES

(1) Taylor, G. I. *Proc. R. Soc. London, Ser. A* **1932**, *138*, 41–48.
(2) Taylor, G. I. *Proc. R. Soc. London, Ser. A* **1934**, *146*, 501–523.
(3) Tucker, C. L.; Moldenaers, P. *Annu. Rev. Fluid Mech.* **2002**, *34*, 177–210.
(4) Guido, S.; Greco, F. In *Rheology Reviews 2004*; Bindong, D. M., Walters, K., Eds.; The British Society of Rheology, 2004; pp 99—142.
(5) Stone, H. A. *Annu. Rev. Fluid Mech.* **1994**, *26*, 65–102.
(6) Rumscheidt, F. D.; Mason, S. G. *J. Colloid Sc.* **1961**, *16*, 238–261.
(7) Tomotika, S. *Proc. R. Soc. London, A* **1936**, *153*, 302–318.
(8) Mikami, T.; Cox, R. G.; Mason, S. G. *Int. J. Multiphase Flow* **1975**, *2* (2), 113–38.
(9) Khakhar, D. V.; Ottino, J. M. *J. Fluid Mech.* **1986**, *166*, 265–285.
(10) Stone, H. A.; Bentley, B. L.; Leal, L. G. *J. Fluid Mech.* **1986**, *173*, 131–158.
(11) Stone, H. A.; Leal, L. G. *J. Fluid Mech.* **1989**, *198*, 399–427.
(12) Stone, H. A.; Leal, L. G. *J. Fluid Mech.* **1989**, *206*, 223–263.
(13) de Bruijn, R. A. Ph.D. Thesis, Eindhoven University of Technology, Eindhoven, The Netherlands, 1989.
(14) de Bruijn, R. A. *Chem. Eng. Sci.* **1993**, *48* (2), 277–284.
(15) Van Puyvelde, P.; Velankar, S.; Moldenaers, P. *Curr. Opin. Colloid Interface Sci.* **2001**, *6* (5—6), 457–463.
(16) Migler, K. B. *J. Rheol.* **2000**, *44*, 277–290.
(17) Hobbie, K.; Migler, K. B. *Phys. Rev. Lett.* **1999**, *82*, 5393–5396.
(18) Anna, S. L.; Mayer, H. C. *Phys. Fluids* **2006**, art.no. 121512.
(19) Lee, W.; Walker, L. M.; Anna, S. L. *Phys. Fluids* **2009**, art.no. 032103.
(20) Han, C. D.; Funatsu, K. *J. Rheol.* **1978**, *22*, 113–133.
(21) Chin, H. B.; Han, C. D. *J. Rheol.* **1980**, *24*, 1–37.
(22) Van der Reijden-Stolk, C.; Sara, A. *Polym. Eng. Sci.* **1986**, *26*, 1229–1239.
(23) Vananroye, A.; Van Puyvelde, P.; Moldenaers, P. *Langmuir* **2006**, *22* (9), 3972–3974.
(24) Van Puyvelde, P.; Vananroye, A.; Cardinaels, R.; Moldenaers, P. *Polymer* **2008**, *49* (25), 5363–5372.
(25) Godbille, F. D.; Picot, J. J. C. *Adv. Polym. Tech.* **2000**, *19*, 14–21.
(26) Khayat, R. E.; Luciani, A.; Utracki, L. A.; Godbille, F. D.; Picot, J. J. C. *Int. J. Multiphase Flow* **2000**, *26*, 17–44.
(27) Mietus, W. G. P.; Matar, O. K.; Lawrence, C. J.; B.J, B. *Chem. Eng. Sci.* **2002**, *57*, 1217–1230.
(28) Testa, C.; Sigillo, I.; Grizzuti, N. *Polymer* **2001**, *42*, 5651–5659.
(29) Priore, B. E.; Walker, L. M. *J. Rheol.* **2001**, *45*, 383–402.
(30) Oosterlinck, F.; Vinckier, I.; Mours, M.; Laun, H. M.; Moldenaers, P. *Rheol. Acta* **2005**, *44* (6), 631–643.
(31) Bentley, B. L.; Leal, L. G. *J. Fluid Mech.* **1986**, *167*, 241–283.
(32) Ballal, B. Y.; Rivlin, R. S. *Arch. Rat. Mech. Anal.* **1976**, *62* (3), 237–294.
(33) Diprima, R. C.; Stuart, J. T. *ASME J. Lubr. Technol.* **1972**, *94*, 266–274.
(34) Kulinski, E. S.; Ostrach, S. *ASME J. Appl. Mech.* **1967**, *34*, 16–22.
(35) Kusch, H. A.; Ottino, J. M. *J. Fluid Mech.* **1992**, *236*, 319–348.
(36) Ottino, J. M.; Leong, C. W.; Rising, H.; Swanson, P. D. *Nature* **1988**, *333* (6172), 419–425.
(37) Tjahjadi, M.; Ottino, J. M. *J. Fluid Mech.* **1991**, *232*, 191–219.

(38) Feigl, K.; Kaufmann, S. F. M.; Fischer, P.; Windhab, E. J. *Chem. Eng. Sci.* **2003**, *58* (11), 2351–2363.
(39) Egholm, R. D.; Fischer, P.; Feigl, K.; Windhab, E. J.; Kipka, R.; Szabo, P. *Chem. Eng. Sci.* **2008**, 3526–3536.
(40) Windhab, E. J.; Dressler, M.; Feigl, K.; Fischer, P.; Megias-Alguacil, D. *Chem. Eng. Sci.* **2005**, *60* (8—9), 2101–2113.
(41) Boonen, E.; Van Puyvelde, P.; Moldenaers, P. *Rheol. Acta* **2009**, *48*, 359–371.
(42) Janssen, J. M. H.; Meijer, H. E. H. *J. Rheol.* **1993**, *37* (4), 597–608.
(43) Macosko, C. W. *Rheology: Principles, Measurements and Applications*; Wiley: New York, 1994.
(44) Grace, H. P. *Chem. Eng. Commun.* **1982**, *14* (3—6), 225–277.
(45) Van Puyvelde, P. Ph.D. Thesis, Catholic University of Leuven, Leuven, Belgium, 1999.
(46) Van Puyvelde, P.; Yang, H.; Mewis, J.; Moldenaers, P. *J. Rheol.* **2000**, *44* (6), 1401–1415.
(47) Boonen, E.; Van Puyvelde, P.; Moldenaers, P. *J. Rheol.* **2010**, accepted for publication.
(48) Tsakalos, V. T.; Navard, P.; Peuvrel-Disdier, E. *J. Rheol.* **1998**, *42* (6), 1403–1417.
(49) Van Puyvelde, P.; Antonov, Y. A.; Moldenaers, P. *Food Hydrocolloids* **2003**, *17* (3), 327–332.

AM100389X